Research on Different Characteristics of a Cell and the Implementation of Local Alumina Control

Zhibin Zhao[1], Shuzhen Ma[2], Ruisheng Zhang[3], Junfeng Qi[4], Chao Liu[5] and Wei Liu[6]
1.Chief Engineer
4. Research Engineer
6. Director
Science and Technology Management Department, Shenyang Aluminium & Magnesium Engineering & Research Institute, Shenyang, China
2.Vice Manager
3. Senior Engineer
Yunnan Wenshan Aluminum Smelter, Wenshan, China
5. Research Engineer
School of Metallurgy – Northeastern University, Shenyang, China
Corresponding author: wei_liu232@chinalco.com.cn
https://doi.org/10.71659/icsoba2024-al017

Abstract

This paper conducted an analysis on different characteristics in a cell operated by an aluminum smelter. There is a gradient in the distribution of bath temperature, superheat, and alumina concentration in the same cell. Aimed at these different characteristics, an industrial test on the local control of alumina concentration was implemented for 6 months. The results showed that the current efficiency of test cells increased by 0.51 % compared to reference cells, the DC energy consumption decreased by 62 kWh/t Al, and the anode effect frequency was decreased by 40 %. The test showed that the local control technology of alumina is promising, and it will be extended to more cells in aluminum smelters.

Keywords: Aluminum electrolysis cell, Local control of alumina, Industrial testing, superheat.

1. Introduction

During the past century, many significant technological advancements have been made since the invention of Hall-Héroult method. It still is the only way to produce primary aluminum at commercial scale. The aluminum electrolytic cell is the heart of metal extracting, which has experienced a gradual increase in capacity from 4 kA to 600 kA. Now the cell size or capacity stills shows an increasing trend, some authors even discussed the possibility of 1 MA cell [1].

The 500 kA cells discussed in this paper were designed by Shenyang Aluminum & Magnesium Design & Research Institute Co., Ltd. (SAMI), and produce about 500 000 tonnes of aluminum per year. The reaction area (also called bath layer) inside the cell is about 20 meters long, 4 meters wide and 0.20 meters high. In such a huge space, the operation is managed by computer control (cell controller):

1) The cell controller manages the cell voltage or the anode-cathode distance (ACD) by monitoring the change of cell resistance with alumina concentration [2, 3];
2) The alumina is fed by several feeding points distributed along cell, to keep the alumina concentration in the bath in a narrow range of 1.5 % to 3.5 % and thus avoid anode effect and sludge [4].

In recent years with the increase of cell size, especially with the use of 500 kA, 600 kA cells, there are some new problems coming to light. The anode effect control, voltage control (operating voltage - set voltage) and alumina control are getting difficult comparing with previous small

cells. For instance, the possibilities of high anode effect frequency (especially local anode effects) are higher in larger cells than in small cells. An anode effect is declared when the cell voltage becomes greater than 8 V for more than 15 s, while a local anode effect occurs in less than 15 s. Some local anode effects can be terminated automatically, but some can spread to other anodes and grow up to a full anode effect. In this direction, the sensitivity of cells management became one of the hottest topics in these days.

Focused on different characteristics in the same cell, the first part of this paper describes the measured and analyzed distribution of bath temperature, superheat and alumina concentration. The second part was carried out as an industrial test for 6 months to optimize the spatial gradient of alumina concentration. The third part shows some results after the implementation of local alumina control technology.

2. Research on Different Characteristics in the Same Cell

2.1 Bath Temperature and Superheat

Bath temperature and superheat are two key parameters for the cell control in the production of metal. Most previous papers focused on the distribution in different cells [5, 6], ignoring the variability of temperature and superheat distribution in the same cell.

Only 6 cells were selected (Cell No. 1508 to 1513) for temperature and superheat measurements. In order to get more accurate data, some key rules are listed here:

1) Thermocouple probes, used for bath temperature measurement, needed to be calibrated before the test;
2) The thermocouple probes were inserted into the bath at 10 cm to 15 cm from tap-end hole and duct-end hole for the purpose of measuring in the ACD layer. After the temperature measurement, bath samples were quickly scooped out by spoons.
3) The most important rule was to strictly follow the principle of simultaneous temperature measurement and sample scooping at the tap-end hole and duct-end hole.

After the temperature measurements and sampling, the bath samples were sent to the smelter laboratory for liquidus temperature determination. Then the superheat could be calculated as bath temperature minus liquidus temperature. The solidification of the bath is exothermic, reflecting in the temperature curve as an obvious plateau. The temperature of the plateau is the liquidus temperature. The equipment, bath crucible and temperature curve are shown in Figure 1.

Table 1 lists bath temperature and superheat. In order to get data under different cell conditions, three measurements were carried out for each cell in three days (day 1, day 3 and day 5). The average bath temperature at tap-end is 933.7 °C. The average bath temperature at duct-end is 932.3 °C. Bath temperature at the tap-end is 1.4 °C higher than that of the duct-end. The superheat at the tap-end (9.8 °C) is also higher than the value of 9.1 °C at duct-end. Prof. Naixiang Feng summarized in his book [6] that the superheat is usually between 8 °C and 10 °C. It can be seen in Table 1, that the average superheat in six cells is higher than 9 °C both at the duct-end and tap-end, which indicates that the superheat control is good in this smelter.

Table 2 shows the standard normal distribution of superheat. The mean value is 9.8 °C and the standard deviation (σ) is 3.1 °C at tap-end. The mean value is 9.1 °C and the standard deviation (σ) is 4.0 °C at duct-end. It also can be seen that there are some superheats smaller than 5 °C. Considering that bath temperature decreases by 4.7 °C during anode change [7, 8], the alumina may have dissolution issues in the bath near new anodes. Some optimization methods should be carried out for better control of superheat, which may be the work in the future.

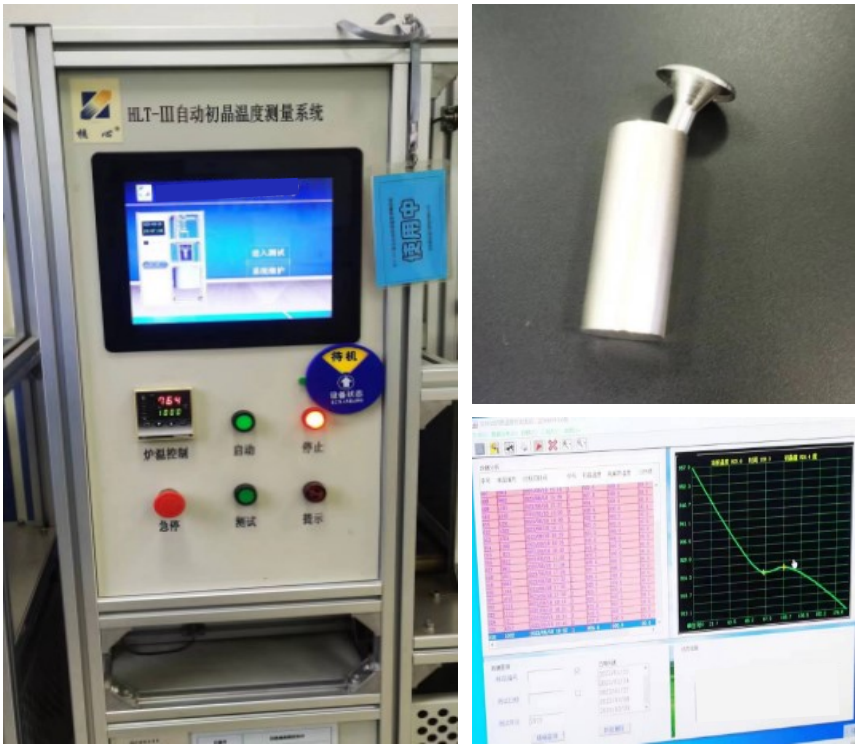

Figure 1. Liquidus temperature measurements.

In table 1, both bath temperature and superheat are slightly higher at tap end than at duct end. It can be speculated that the bath in the half cell of tap-end may have the potential for better alumina dissolution. Table 2 shows the superheat distribution.

Table 1. Measured bath temperature and superheat.

Cell	Temperature (°C)			Superheat (°C)		
	Tap-end	**Duct-end**	**Difference**	**Tap-end**	**Duct-end**	**Difference**
1508_Day1	933.3	934.4	-1.1	13.3	11.3	2.0
1509_Day1	937.5	932.0	5.5	9.7	7.0	2.7
1510_Day1	935.0	933.0	2	10.6	——	——
1511_Day1	937.4	933.0	4.4	8.8	8.3	0.5
1512_Day1	939.4	936.5	2.9	16.4	13.6	2.8
1513_Day1	931.2	937.8	-6.6	11.2	16.3	-5.1
1508_Day3	931.7	931.7	0	9.0	12.9	-3.9
1509_Day3	933.7	932.3	1.4	3.7	3.9	-0.2
1510_Day3	925.0	924.5	0.5	——	3.4	——
1511_Day3	932.3	931.2	1.1	8.5	3.2	5.3
1512_Day3	935.2	933.0	2.2	5.6	12.3	-6.7
1513_Day3	932.2	929.3	2.9	10.4	11.3	-0.9
1508_Day5	928.4	927.5	0.9	7.3	4.8	2.5
1509_Day5	941.6	940.6	1.0	13.0	12.3	0.7
1510_Day5	931.8	933.0	-1.2	12.1	12.1	0
1511_Day5	936.5	931.2	5.3	11.3	6.1	5.2
1512_Day5	932.5	932.0	0.5	7.0	8.9	-1.9
1513_Day5	932.0	927.8	4.2	8.4	6.6	1.8
AVE	933.7	932.3	1.4	9.8	9.1	0.7
STDEV				3.1	4.0	-0.9

Table 2. Standard normal distribution of superheat.

Superheat (SH) distribution			
Tap-end		**Duct-end**	
SH ≤ μ - 2σ	0.0 %	SH ≤ μ - 2σ	0.0 %
μ - 2σ < SH ≤ μ - σ	11.8 %	μ - 2σ < SH ≤ μ - σ	23.5 %
μ - σ < SH ≤ μ	41.2 %	μ - σ < SH ≤ μ	29.4 %
μ < SH ≤ μ + σ	29.4 %	μ < SH ≤ μ + σ	35.3 %
μ + σ < SH ≤ μ + 2σ	11.8 %	μ + σ < SH ≤ μ + 2σ	11.8 %
μ + 2σ < SH	5.9 %	μ + 2σ < SH	0.0 %
μ - σ < SH ≤ μ + σ	**70.6 %**	**μ - σ < SH ≤ μ + σ**	**64.7 %**
μ - 2σ < SH ≤ μ + 2σ	**94.1 %**	**μ - 2σ < SH ≤ μ + 2σ**	**100.0 %**

2.2 Alumina Concentration

The bath samples were scooped out and the alumina concentration of these samples is analyzed in this section. Two cells (Cell No. 1508 and 1509) were chosen here for the alumina concentration measurement. The sampling points and process are shown in Figure 2 and Figure 3. Sampling point 1 (SP1) was the tap-end hole. SP2 was located in side channel between anode A3 and A4 in upstream side (also called side A), SP3 was the hole between anode A15 and anode A16. SP4 was the duct-end hole. There were two more sampling points along the downstream side (side B), SP5 and SP6. During the test, the simultaneous sampling rule was also strictly followed.

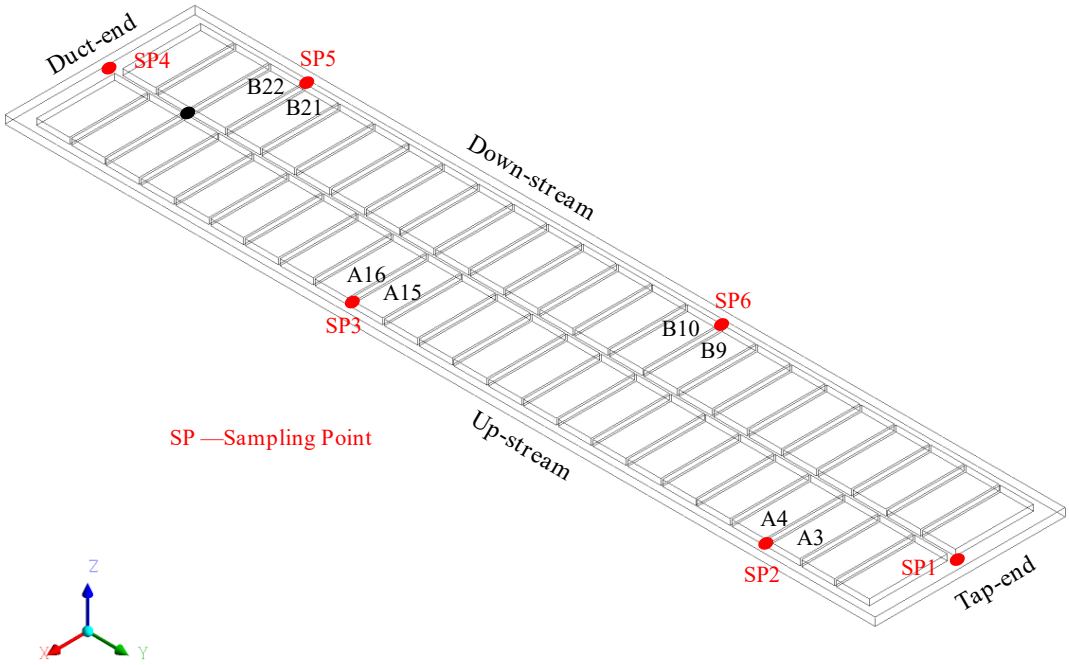

Figure 2. Schematic diagram of sampling points.

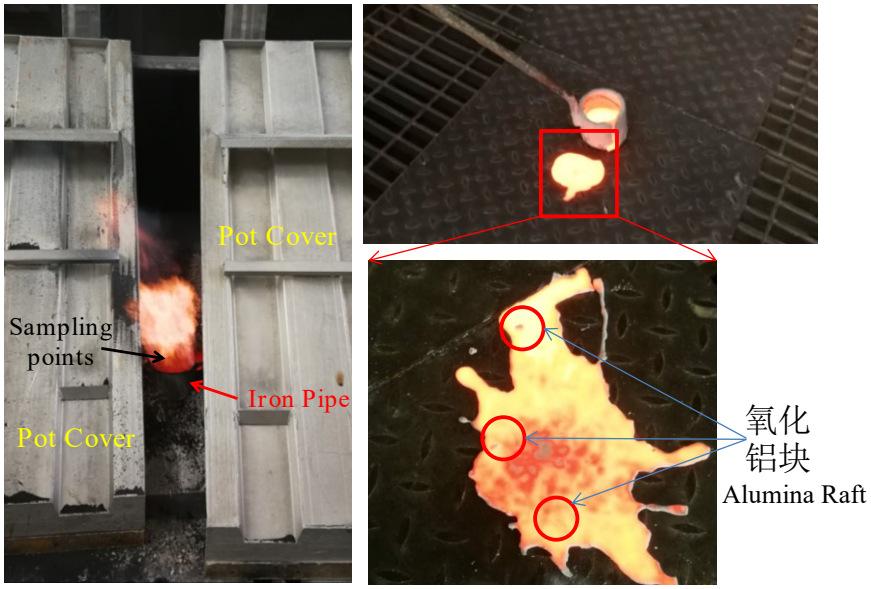

Figure 3. Sampling process.

A total of 72 samples (12 sets of samples named S1 to S12, each with 6 samples) were obtained in the operating Cell No. 1509, and the alumina concentration was chemically analyzed in the laboratory. Figure 4 shows the sampling time and results of the alumina concentration measurement. It also shows the average alumina concentration during two overfeeding and one underfeeding period. The alumina concentration ranges from 1.6 % to 1.8 %, coinciding with the variation of cell voltage.

Figure 4. Sampling time and results of alumina concentration test.

Based on the comparison of data in Table 3 and points shown in Figure 2, it can be found that SP3, SP4, and SP5, which are located in the half cell near the duct-end, have an average concentration of 1.62 %. SP1, SP2, and SP6, which are located in the half-cell near the tap-end, have an average concentration of 1.72 %. The concentration of the right half-cell is greater than

that of the left half-cell. The same phenomenon of alumina concentration was observed in the second sampling measurement in 1509 and other measurements of 1508. This is the same conclusion as speculated in the previous section through temperature and super heat analysis.

The analytical result of alumina measurement is different with the results shown in another 500 kA cell described in the literature [9]. This may be related to the busbar designs, cell designs, or other factors. It will be further investigated in the future to address this issue.

Table 3. Alumina concentration measurements (1) (%).

1509-Al_2O_3		SP1	SP2	SP3	SP4	SP5	SP6	AVE	DE-HALF	TE-HALF
S-1	1	1.94	1.90	1.50	1.59	1.58	1.42	1.66	1.56	1.75
S-3	3	2.12	1.57	1.62	1.33	1.62	1.48	1.62	1.52	1.72
S-4	4	1.98	1.74	1.41	1.48	1.66	1.42	1.62	1.52	1.71
S-6	6	2.17	1.84	1.50	1.46	1.80	1.44	1.70	1.59	1.82
S-8	8	1.76	1.96	1.85	1.98	1.78	1.48	1.80	1.87	1.73
S-10	10	1.76	1.83	1.74	1.46	1.70	1.46	1.66	1.63	1.68
S-12	12	2.14	1.82	1.68	1.46	1.83	1.44	1.65	1.66	1.63
AVE		1.98	1.81	1.61	1.54	1.71	1.45	AVE	1.62	1.72

3. Alumina Concentration Control

The previous section showed that there is a gradient in the distribution of bath temperature and superheat in the same cell, which is reflected by the gradient in the distribution of alumina concentration. Now, very limited works have considered this variability and its related impact in the cell. Focused on these different characteristics, this section describes an industrial test on local control of alumina concentration for 6 months.

3.1 Local Control of Alumina Concentration

The so-called local control of alumina concentration is to divide the electrolytic cell into a number of sub-regions, then the alumina concentration of each region is individually monitored by technical means, and accurately controlled by single point feeding. In this test, the cell was divided into 6 sub-regions according to the number of feeding points as shown in Figure 5. The local control was carried out based on the alumina feeding, transport and consumption to manage the customized feeding. The logic of local control can be described by the following equation.

$$C_t = C_{t-1} + C_{in} + C_{out} + f(I_i) \quad (1)$$

where:

C_t Alumina concentration in the region at the current moment.
C_{t-1} Alumina concentration in the region at the previous moment.
C_{in} Alumina concentration flowing into the region.
C_{out} Alumina concentration flowing out of this region.
$f(I_i)$ Rate of alumina consumption associated with the individual anode current distribution.

Based on the logic, the uneven feeding rate of the 6 feeders was made, instead of the previous average feeding policy. The individual anode current is shown in Figure 6. The local control can be seen as an active control for the gradient of alumina concentration in the cell.

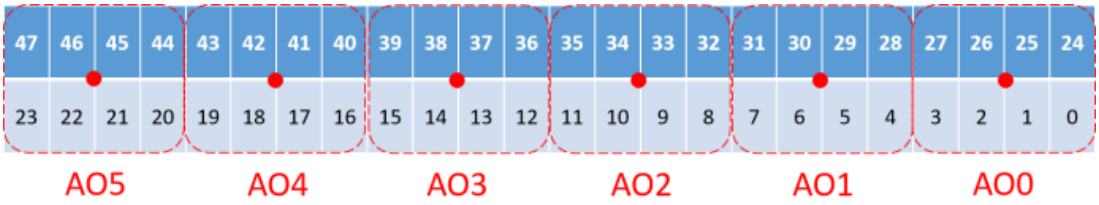

Figure 5. Sub-regions of the cell for local control of alumina concentration.

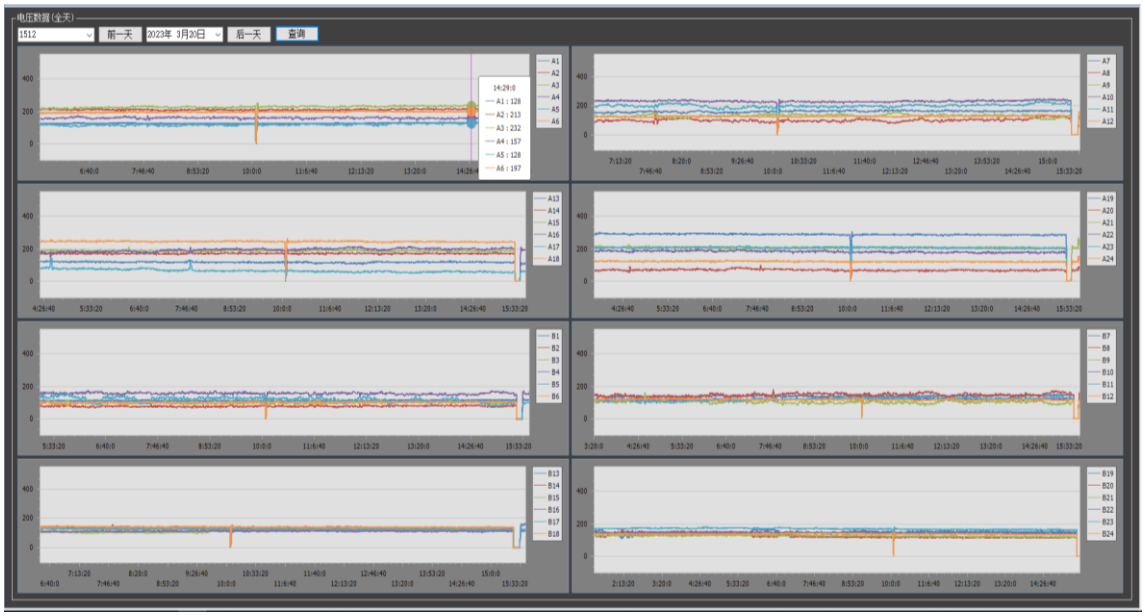

Figure 6. The distribution of individual anode currents.

3.2 Anode Effect Detection and Termination

Anode effects are always associated with a depletion of alumina, and at low alumina concentration the wettability of electrolyte and carbon anode is getting poor and results in bubble evacuation problems. The anode effect usually starts from one individual anode or a part of an individual anode, and then spreads to more anodes throughout the cell. In the traditional anode effect detection, the cell voltage suddenly and substantially increases (Figure 7a). Looking at individual anode currents, the current of an anode that is to have an anode effect is quickly redistributed to other anodes. This can be used to detect and anode effect before it occurs (Figure 7b) [10].

In this section, an algorithm for anode effect detection and termination was developed based on the individual anode current signals. Figure 8 shows the individual anode current before the anode effect occurs. The current of anode A1 (A1_ORG) decreases rapidly before the anode effect occurs. The filtered anode current (A1_FIT) is illustrated using filtering method, and then the anode current slope calculation (dI/dt) is performed. From the slope (A1_Slope), the anode effect can be detected 120 s to 300 s before it occurs. The single point feeding technique then is used to give breaking and alumina shots near the troubled anodes.

The anode effect detection and termination can be regarded as a passive control for the gradient of alumina concentration in the cell.

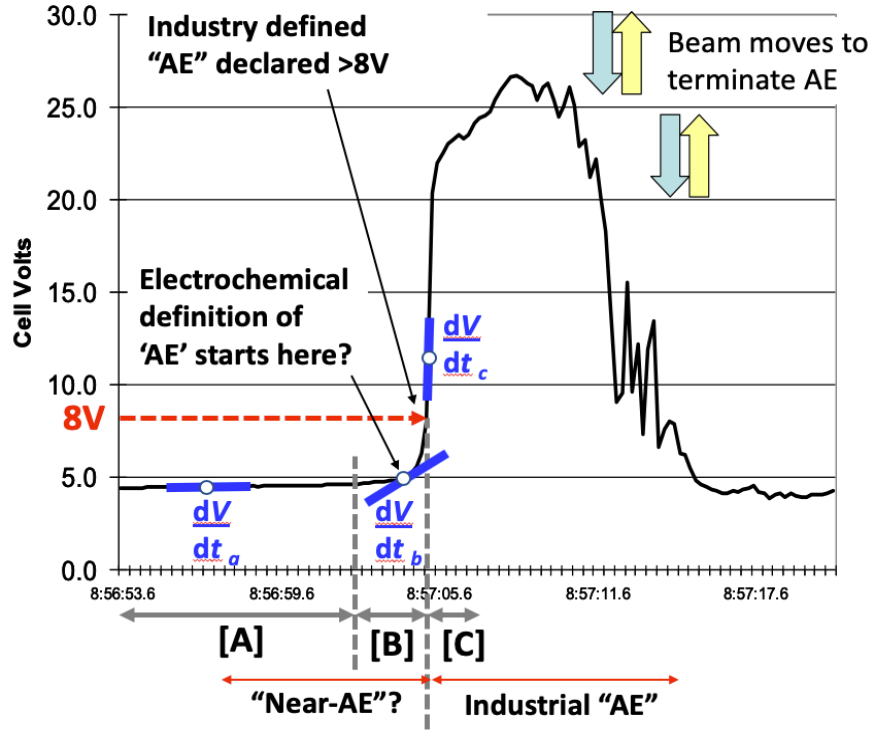

(a)

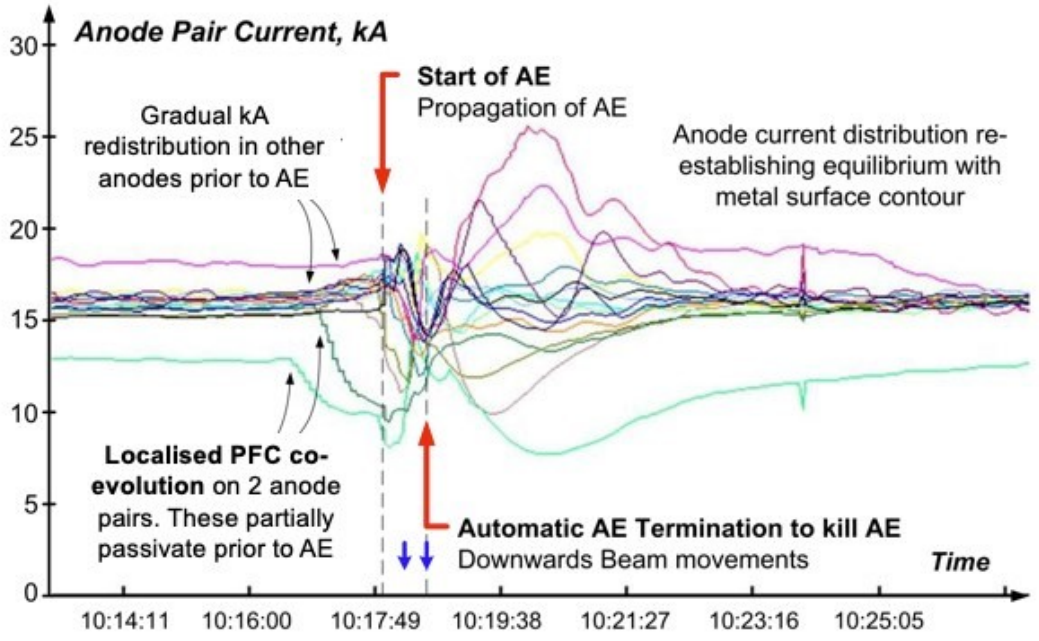

(b)

Figure 7. The anode effect detection logic in traditional cell controller and individual anode current. Top: (a) Voltage signature of an anode effect on a 220 kA cell; Bottom: (b) Individual anode currents before, during and after an anode effect [10].

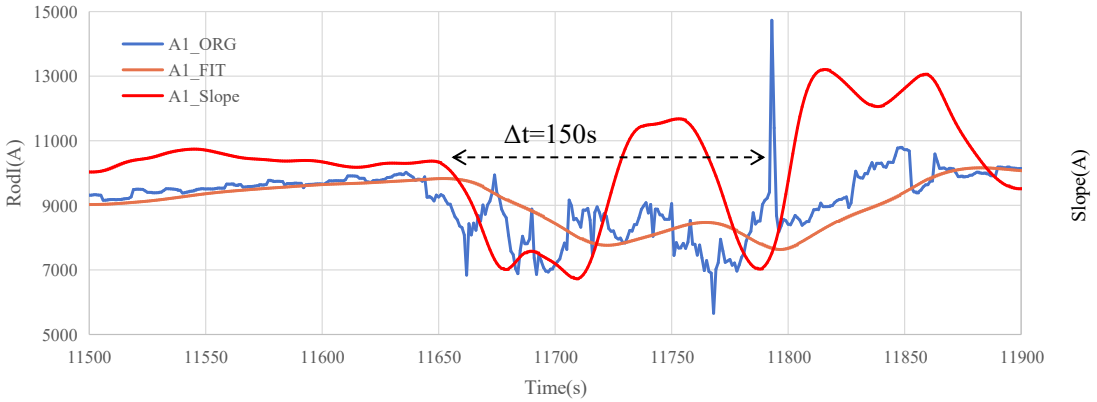

Figure 8. Individual anode currents before, during and after an anode effect.

4. Effect of Local Control of Alumina Concentration

Figure 9 shows the effects of local control of alumina concentration, and anode effect detection and termination. There was a successful anode effect termination and a failed anode effect termination in one day. For the successful case, the alumina was shot into the cell two times after the anode effect detection (total alumina is 2 × 1.8 kg), and the anode effect (or local anode effect) was killed. While in the failed case, the anode effect was still present even if the alumina was added four times (total alumina 4 × 1.8 kg).

A new alumina measurement was carried out after one month of the implementation of local control (Table 4), the average alumina concentration in the half-cell near duct end was 1.80 % and it was 1.82 % on the other half cell (shown in Table 4).

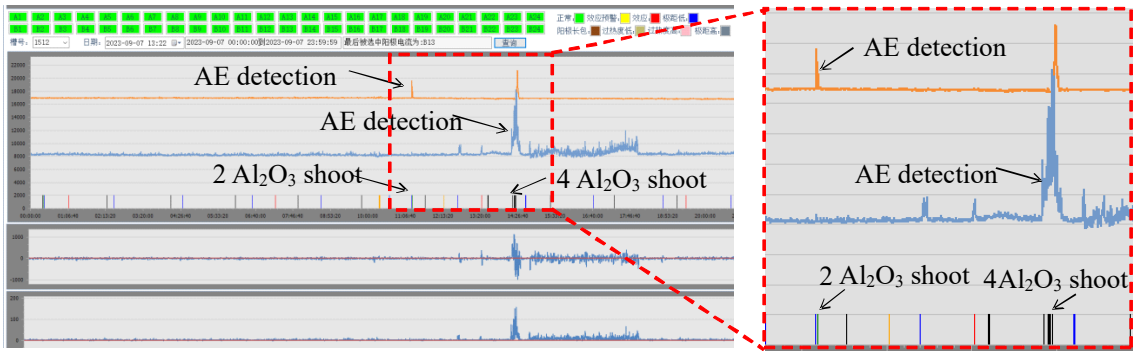

Figure 9. The local control of alumina concentration.

Table 4. Alumina concentration measurements (2) (%).

1509-Al_2O_3		SP1	SP2	SP3	SP4	SP5	SP6	AVE	TE-HALF
S-1	1	2.03	1.84	1.79	1.86	2.02	1.77	1.89	1.88
S-3	3	2.06	1.78	1.88	1.68	1.80	1.63	1.81	1.82
S-4	4	1.98	1.67	1.65	1.68	1.76	1.72	1.74	1.79
S-6	6	1.88	1.65	1.66	1.73	1.71	1.68	1.72	1.74
S-8	8	2.10	1.85	1.83	1.66	1.72	1.73	1.82	1.89
S-10	10	1.83	1.81	1.94	1.76	1.98	1.74	1.84	1.79
S-12	12	2.12	1.84	1.91	1.91	1.78	1.85	1.86	1.85
AVE		2.00	1.78	1.81	1.75	1.82	1.73	AVE	1.82

The industrial test was carried out on the 6 cells for 6 months. The test cells were cells No. 1508 to 1513, while the reference cells were the other 41 cells in the same section. This test was started on 1 May 2023 and ended on 31 October 2023. The reference period was from 1 February 2023 to 30 April 2023.

4.1 Current Efficiency

Figure 10 shows the comparison of current efficiency before and after the test of local control technology. The average current efficiency of test cells from May to October 2023 was 94.14 %, an increase of 1.25 % compared with the average value from January to April (92.89 %). The average current efficiency of reference cells from May to October 2023 was 93.42 %, an increase of 0.74 % compared with the value from January to April (92.68 %).

In summary, the current efficiency was increased by 0.51 % due to the local control during the test.

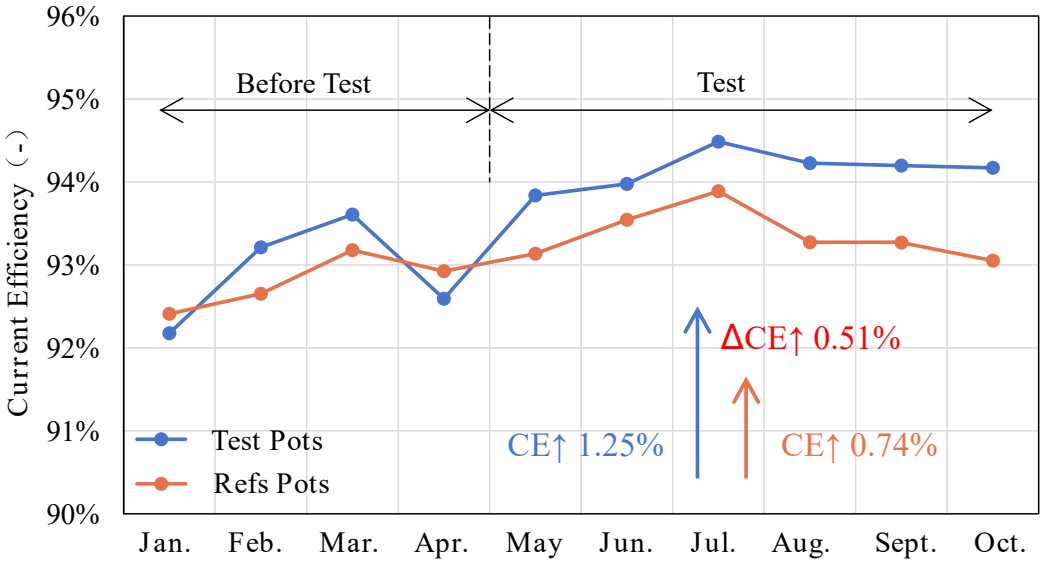

Figure 10. Comparison of current efficiency before and after the test.

4.2 DC Energy Consumption

Figure 11 shows the comparison of DC energy consumption before and after the local control technology. The average DC energy consumption of test cells from May to October 2023 (12 537 kWh/t Al) is 199 kWh/t Al lower than that from January to April 2023 (12 736 kWh/t Al). The average DC energy consumption of the reference cells from May to October 2023 (12 682 kWh/t Al) is 137 kWh/t Al lower than that from January to April 2023 (12 819 kWh/t Al). In summary, the DC energy consumption was decreased by 62 kWh/t Al due to the local control during the test.

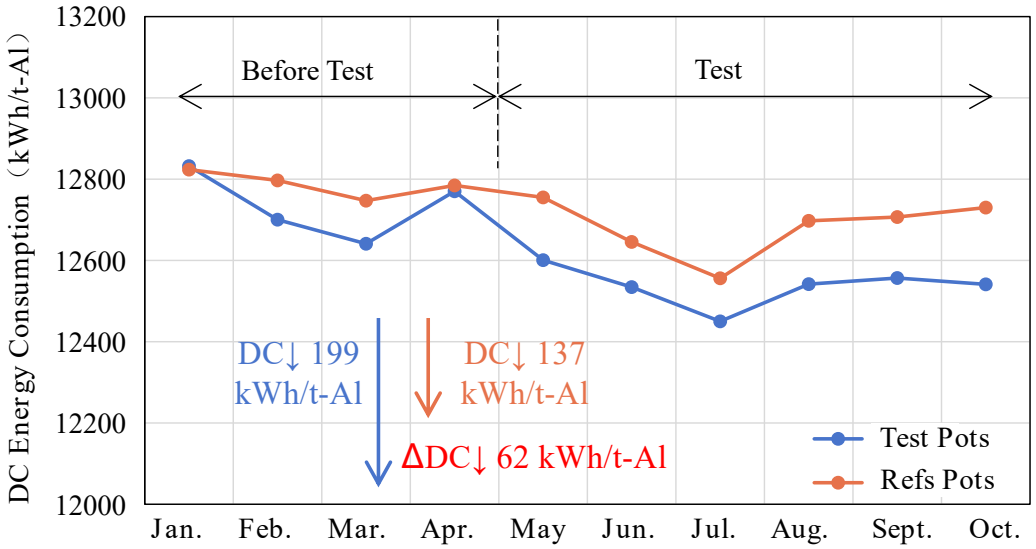

Figure 11. Comparison of DC energy consumption before and after the test.

4.3 Anode Effect Frequency

The average anode effect frequency of reference cells during the test was 0.05 AE/cell·day. The average anode effect frequency of test cells was 0.03 AE/cell·day, which was 40 % lower than the anode effect frequency of reference cells at the same time.

5. Conclusions

(1) Different characteristics of a 500 kA cell were measured in this paper. Bath temperature, superheat and alumina concentration in the half-cell near tap-end are slightly higher than that near the duct-end. A six-month industrial test was carried out to fix this problem.

(2) The local control of alumina concentration was put forward to optimize the spatial gradient. The cell was divided into six sub-regions, and the alumina was monitored and controlled individually in each region according to alumina feeding, transport and consumption. This is an active control for the gradient of alumina concentration.

(3) The individual anode current was used for anode effect detection and termination. The anode effect can be detected 120 s to 300 s before it occurs. The single point feeding technique then is applied for one break or one shot of alumina near the troubled anode. This is a passive control for the gradient of alumina concentration.

(4) Through the implementation of local control in 6 months, the current efficiency of test cells was increased by 0.51 %, the DC energy consumption was reduced by 62 kWh/t Al, and the anode effect frequency was reduced by 40 %. The test showed that the local control is promising, and it will be extended to more cells in the aluminum smelters.

6. References

1. Marc Dupuis and Barry Welch, Designing cells for the future–Wider and/or even higher amperage?, *ALUMINIUM*, 2017, 1 - 2.

2. Vinko Potocnik and Michel Reverdy, History of computer control of aluminum reduction cells, *Light Metals* 2021, 591-599.
3. Xiaodong Yang and Ming Liu, Innovative ideas on heat balance design of large energy-saving aluminum reduction cell, *Light Metals*, Vol. 12, (2017), 21-25. (in Chinese)
4. Wei Liu, Hongsheng Hu, Dong Zhou, et al., Numerical modeling of bath-bubble two phase flow and alumina mixing in aluminum reduction cell, *Light Metals*, Vol. 1, (2016), 25-29. (in Chinese)
5. Youshan Wang, Xuemin Liang, Xiaodong Kang, et al., Analysis on the electrolytic temperature and super-heat degree of large aluminum reduction cell, *Light Metals*, Vol. 12, (2012), 35-38. (in Chinese)
6. Naixiang Feng, *Aluminum electrolysis*, 1st Edition, Beijing, Chemical Industry Press, 2006, 125 pages.
7. Zhibin Zhao, Wei Liu, Yafeng Liu, et al., A discussion on thermal impact of anode change in aluminum reduction cell, *Light Metals* 2023, 128-136.
8. Zhibin Zhao, Wei Liu, Qinsong Liu, et al., Impact of anode change on MHD in aluminum reduction cell, *Proceedings of 41th International Conference of ICSOBA*, 5–9 November 2023, Dubai, United Arab Emirates, *TRAVAUX* 52, 1711–1724.
9. Jiamin Zhu, Jie Li and Hongliang Zhang. CFD investigation of bath flow and its related alumina transmission in aluminum reduction cells: slotted anodes and busbar designs. *Metals*, Vol. 10, 2020, 805-820.
10. David Wong, Barry Welch, Pernelle Nunez, et al., Latest progress in IPCC methodology for estimating the extent of PFC greenhouse gases co-evolved in the aluminium reduction cell and challenges in reducing these emissions, *Proceedings of 37th International Conference of ICSOBA and XXV International Conference "Aluminium of Siberia"*, 16–20 September 2019, Krasnoyarsk, Russia, *TRAVAUX* 48, 735–758.